Volume 20
Number 14
14 April 2024
Pages 3025–3204

Soft Matter

rsc.li/soft-matter-journal

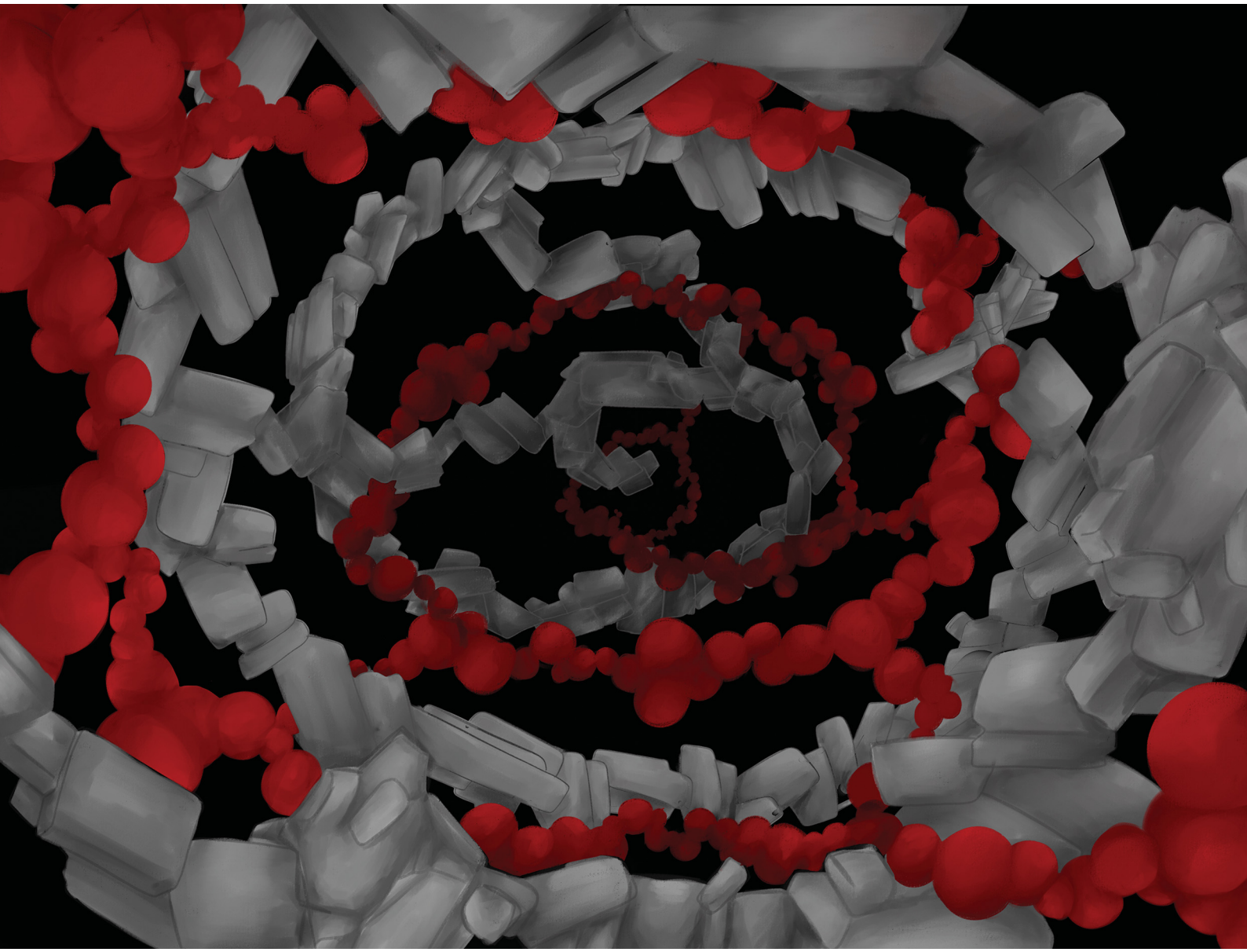

ISSN 1744-6848

ROYAL SOCIETY OF CHEMISTRY

PAPER

Braulio A. Macias-Rodriguez, Krassimir P. Velikov *et al.*
Thermoresponsive oil-continuous gels based on double-interpenetrating colloidal-particle networks

Soft Matter

PAPER

View Article Online
View Journal | View Issue

Check for updates

Cite this: *Soft Matter*, 2024, **20**, 3033

Thermoresponsive oil-continuous gels based on double-interpenetrating colloidal-particle networks†

Braulio A. Macias-Rodriguez, ‡*[ab] Roland Gouzy,[ab] Corentin Coulais [b] and Krassimir P. Velikov *[abc]

Gels composed of multicomponent building blocks offer promising opportunities for the development of novel soft materials with unique and useful structures. While interpenetrating polymer networks have been extensively studied and applied in the creation of these gels, equivalent strategies utilizing colloidal particles have received limited scientific and technological attention. This study presents a novel class of thermo-responsive apolar double gels from interpenetrating networks of attractive colloidal silica and lipid particles. These double gels are easily assembled and suitable for the fabrication of 3D-printed edible soft constructs. Emphasis is focused on the rheological properties and structure emerging on the dilute regime ($\phi \lesssim 0.1$). Rheological investigations demonstrate that double gels exhibit greater stiffness and resilience to yielding compared to their single lipid gel counterparts. The scaling behavior of the oscillatory linear shear moduli and the critical strain for yielding with volume fraction remain comparable between single and double gels. Creep yielding in double gels exhibits two exponential decay regimes, suggesting the presence of thicker gel strands undergoing flow. Visualization and quantification of the quiescent microstructure confirms the existence of such denser aggregates devoid of larger clusters due to steric hindrance of interpenetrating networks in double gels. This is in stark contrast to lipid single gels where aggregates grow unrestrictedly into larger clusters. Our study constitutes the first demonstration on the assembly of apolar double gel networks as a promising avenue for the design of novel soft materials and foods with tailored structure and mechanics.

Received 21st November 2023,
Accepted 8th February 2024

DOI: 10.1039/d3sm01582c

rsc.li/soft-matter-journal

Published on 08 February 2024. Downloaded on 4/11/2024 2:11:41 PM.

Introduction

Gelation is observed in a broad spectrum of colloidal suspensions. These suspensions contain particles at low-to-intermediate concentrations, exhibiting an interparticle attractive potential. Due to its ubiquity, addressing fundamental questions about the origin of the colloidal gel state and elucidating the interplay between structure and internal dynamics is crucial for controlling the properties of soft materials.[1] These materials are found in ceramics, films, cosmetics, paints and coatings, pharmaceuticals, foods, *etc.*[1] Several routes to colloidal gelation have been proposed. These include non-equilibrium kinetic arrest *via* spinodal decomposition, kinetic arrest based on competing short-range attractive depletion and long-range electrostatic repulsion, equilibrium arrest induced by highly anisotropic and limited interactions, and other combinations of aggregation pathways.[1–3]

The most extensively studied form of colloidal gel is derived from the non-equilibrium kinetic arrest of a suspension of single monodisperse colloids displaying interparticle attractive interactions. These interactions stem from a variety of sources such as van der Waals forces, surface chemistry, hydrophobic and depletion interactions. They are tuned by additives such as electrolytes, surfactants, polymers, and processing parameters like temperature, pH. The primary types of gels belonging to

[a] *Unilever Innovation Center Wageningen, Bronland 14, 6708 WH Wageningen, The Netherlands. E-mail: bmaciasr@illinois.edu, krassimir.velikov@unilever.com*
[b] *Institute of Physics, University of Amsterdam, Science Park 904, 1098 XH Amsterdam, The Netherlands*
[c] *Soft Condensed Matter, Debye Institute for Nanomaterials Science, Utrecht University, Princetonplein 5, 3584 CC Utrecht, The Netherlands*

† Electronic supplementary information (ESI) available: Mechanics: rheology: temperature sweep, strain sweep at selected volume fractions, storage moduli, yield strain and stress as a function of volume fraction of single gels and double gels. Flow curve of silica single gels. Delayed yielding at higher volume fraction. Compression: strain-stress curves from compression experiments of single gels and double gels. Image acquisition and processing: PLM at increasing of single and double gels at increasing volume fractions. Confocal images of double gels at higher volume fractions and characteristic length scale of silica gels. Small-angle X-ray diffraction of tripalmitin single gels and double gels at selected volume fractions. See DOI: https://doi.org/10.1039/d3sm01582c

‡ Present address: Department of Food Science and Human Nutrition, University of Illinois Urbana-Champaign, 905 S Goodwin Ave, Urbana, IL 61801, USA.

Published on 08 February 2024. Downloaded on 4/11/2024 2:11:41 PM.

this category are model monodisperse systems such as silica, alumina, colloid–polymer systems with infinite or weaker attractions. These gels typically aggregate between the regimes of diffusion limited cluster aggregation and reaction limited cluster aggregation.[2,4] The result of these processes is the same: a disordered stress-bearing scale-invariant network intertwined with a viscous solvent. Under suitable experimental conditions, self-similar microstructures are also encountered in a wide variety of more complex food colloids such as lipid and protein particles.[5–7] Despite not necessarily sharing the same type and strength of interactions as single model colloids, similar phenomenological theories have been applied to both (although not without certain limitations).[6–10] Average descriptions of the self-similar space-filling network have been correlated with the linear elastic modulus using fractal theories.[7,9–13] Notably, these theories are agnostic to the shape of the constituent particle. While such ''universal'' theories have proven fruitful in understanding bulk rheology from microscopic structures, they also reveal limitations on the design space of colloidal gels. For example, the universality of the elasticity of monodisperse colloidal gels of dilute spheres constrains their microstructures to nearly constant fractal dimensions and backbone anisotropy. This leaves bond strength, particle size and particle volume fraction as the only design parameters.[14] In practice, manipulating these variables implies higher concentrations of additives, longer gelation time and larger volume fractions, which are impractical tools from a technological standpoint.[14] Similarly, the rheology of gels made of complex food colloids relies on elaborate and high-energy external field such as temperature, shear, and pressure, to determine the final organized structure.[6,15]

To overcome these limitations, novel colloidal gels based on shape anisotropy, rough surface, patchy colloids, have been proposed as promising avenues to expand the design space of colloidal gels.[14,16–18] Particles with large shape anisotropy aspect ratio, such as LAPONITE® platelets, boehmite rods, and colloidal discoids, can induce significant increases in gel elasticity, in comparison to single spherical colloids due to multiplicative factors acting on the fractal cluster microstructure.[14] The inclusion of rough core–shell silica colloids can also enhance gel toughness by hindering aggregate deformation, in contrast to gels of smooth particles.[16] Patchy colloids can realize arbitrary structures akin to biological proteins.[17] Despite their potential, these systems also present significant challenges, including the need for novel synthesis routes, production in larger quantities, exquisite geometry and surface design to control interactions, anisotropic non-uniform packing, slow gelation, non-uniform stress distribution, among other considerations.[1,14,18]

Importantly, recently developed multicomponent gels, formed, for example, by combining two or more types of selective interparticle interactions, present an exciting alternative for tuning the microstructure of colloidal gels.[19–23] Their composite nature enables individual control of particle interactions and chemistry. Unfortunately, only a limited number of experimental and theoretical studies have been conducted to demonstrate the feasibility of multicomponent gels and investigate in detail their mechanics.[21,23,24] Particularly, in binary mixtures of colloidal particles with selective interparticle interactions (*e.g.*, in DNA-coated colloids, microgels), both experiments and theory highlight a rich plethora of structures (*e.g.*, double gel networks, core–shell networks) and rheological properties (*e.g.*, softening, toughening, stiffening). Although structurally different, the reported rheology appears to share essential features with the well-explored interpenetrating polymer networks utilized for the creation of tough hydrogels for diverse technological uses.[25–31]

In this paper, we present the first realization of double gel networks by mixing two types of colloidal particles that form space-spanning networks of clusters dispersed in a nonpolar solvent, oil. These networks are created through the spontaneous self-assembly of primary asymmetric building blocks: spherical-like fumed silica ($R_g \approx 13 \pm 10$ nm) and platelet-like lipid ($R_g \approx 440 \pm 30$ nm) particles, which display short-range attractive interactions. The gel networks encompass a range of length-scales from approximately 10 nm to 100 μm.[4,32] We select these particles as model colloidal systems due to their thermoresponsiveness and their selective short-range interactions,[4,32,33] which enable the formation of sequentially assembled double colloidal gel networks, and their widespread use in soft materials including in foods. Considering that industries strive to produce sustainable gels with specific rheology at the lowest particle concentrations, we place particular emphasis on colloidal gelation at low levels ($\phi \lesssim 0.1$). To showcase the potential of our systems in technological applications, we use double gels for the fabrication of three-dimensional printed soft constructs, which exhibit exceptional resolution and structural consistency.

To probe the dynamics and microstructure of double gels compared to single particle gels as a function of volume fraction, we use shear rheology and confocal microscopy. Remarkably, our results indicate that double gels can display larger modulus and enhanced yielding dynamics over a broad stress range compared to their lipid single gels counterpart at similar volume fractions. Double gels exhibit denser microstructures characterized by smaller characteristic cluster sizes than lipid single gels, due to the pre-existing silica gel network that sets the spatial length scale of the sequentially aggregated lipid gel network. These unexpected stiffening and stress-enhancement during yielding suggest cooperative effects between the non-mutually attractive gel networks arising due to steric hindrance and limited particle aggregate mobility during shear. Ultimately, these attributes could find broad applications in apolar gel systems, particularly in the realm of fat mimetics.[6]

Experimental section

Materials

Soybean oil (S7381), composed of liquid triglycerides such as trilinoleic was obtained from Sigma-Aldrich. Solid tripalmitin (T8127) was obtained from Sigma-Aldrich. Hydrophilic fumed silica Aerosil® 300, is obtained from Evonik and manufactured

 This journal is © The Royal Society of Chemistry 2024

Published on 08 February 2024. Downloaded on 4/11/2024 2:11:41 PM.

from a flame pyrolysis process that ultimately leads to the formation of silicon dioxide agglomerates.

Silicon dioxide is used as a food additive and is considered non-toxic at the reported typical usage levels of 1.3–5.3% w/w.[34,35] The densities of the materials were 0.92 g cm^{-3} at 25 °C (soybean oil), 0.8901 g cm^{-3} at 47 °C (supercooled tripalmitin)[36] and 2.2 g cm^{-3} (fumed silica).[32]

Preparation of gels

The first gel network consists of fumed colloidal silica with small primary particles ($R_g \approx 13 \pm 10$ nm) that form aggregates due to diffusion-limited growth and then agglomerates of hyperbranched mass fractal structures due to reaction-limited aggregation. In nonpolar solvents, *e.g.*, hydrocarbon and vegetable oils, silica particles exhibit attractive van der Waals interactions, solvation and hydrogen bonding forces that cause them to aggregate, and arrest into an amorphous fractal gel network.[37] The second gel network comprises tripalmitin ($R_g \approx 440 \pm 30$ nm) molecules which below their solid–liquid phase transition temperature T_m ($\sim$48–58 °C depending on volume fraction) condense into primary crystal nanoplatelets that aggregate into an amorphous fractal gel network.[6] In both colloidal gel networks with continuous non-polar solvents, Hamaker coefficients are in the order of $\sim 10^{-20}$ J.[38,39] Upon heating above the solid–liquid phase transition T_m, triglyceride crystal networks melt and dissolve in the continuous oil phase, losing their structural integrity. Whereas, quenching sufficiently below T_m, produces a stress-bearing colloidal network. Silica single gels were prepared by dispersing fumed silica at increasing volume fractions ϕ_{silica} in soybean oil with a high-shear rotator operated at a maximum speed of 17 500 rpm for $t = 5$ min (~ 8 m s^{-1} tip speed for a 10 mm fixture). Lipid single gels were prepared by dispersing solid tripalmitin, heating to 75 °C and holding at the same temperature to melt and erase any remaining 'crystal memory'. Samples were then quenched to 5 °C to provide the driving force for the melt-crystal phase transition. Double gels were prepared by first dispersing a fixed volume fraction of fumed silica $\phi_{silica} = 0.01$ in soybean oil (equivalent to 3% w/w) as described for silica single gels. The fixed low volume fraction of silica, within the acceptable range for food applications, was selected to favor the formation of a primary network with sufficient free volume that allows the assembly of a secondary interpenetrating network.[40]

Molten tripalmitin (75 °C) was then added to the preformed silica gel at increasing volume fractions $\phi_{tripalmitin}$, and held at 75 °C for $t = 5$ min to erase any remaining 'crystal memory'. Mixtures were then quenched as described for lipid single gels. All samples were kept at room temperature (21–22 °C) for a week to ensure complete gelation. Approximate volume fractions for fumed silica ϕ_{silica} and tripalmitin $\phi_{tripalmitin}$ were obtained using densities of the materials. Total volume fraction of single gels and double gels are expressed as ϕ in all figures. Likely sources of uncertainty in the estimation of volume fraction arise due to lower densities for high surface area silica nanoparticles, the ability of fumed silica aggregates to occlude a large amount of oil contributing to higher effective volume fraction, volume fraction of solid tripalmitin which is dependent on the density of the crystallizing polymorphic form, in addition to other systematic errors linked to the estimation of volume fractions in colloids.[41] Gels were formulated at dilute particle concentrations ($\phi \lesssim 0.1$) and at concentrated particle concentrations ($\phi \gtrsim 0.1$). Silica gels were only investigated at dilute particle concentrations ($\phi \lesssim 0.1$) as dispersion in oil at higher volume fractions was not possible. Attention was focused on the properties and structure emerging on the dilute regime ($\phi \lesssim 0.1$), due to the need to create novel gels using colloidal materials at extremely low levels. Experimental data from the concentrated regime, although in a limited concentration range ($\phi \approx 0.1$–0.2) is summarized in the ESI.†

3D-printing of gels

Representative gels were printed at fixed total volume fraction $\phi = 0.10$ at room temperature using a 3D-bioplotter printer (envisionTEC) equipped with an extrusion nozzle of 440 μm. Prior to 3D printing, gels were prepared as described earlier and transferred to the printing syringe. For compression tests, single gels and double gels were printed into solid cylindrical shape specimens measuring 10 mm length by 10 mm diameter ($L/D = 1$).

Structural characterization

Powder X-ray diffraction

X-ray diffraction experiments were conducted to probe any differences in atomic and molecular level packing of tripalmitin tryglycerides and nanoplatelets resulting from the presence of the pre-existing silica gel network. Small-angle X-ray diffraction (SAXD) and Wide-angle X-ray diffraction (WAXD) were conducted on a laboratory scale Bruker D8 Discover X-ray powder diffractometer with a Väntec 500 2D detector and an IμS microfocus X-ray source (CuKα radiation, $\lambda = 0.154184$ nm). The diffraction patterns were collected in a transmission mode with the X-ray beam perpendicular to the flat sample surface. A 1-mm collimating slit was used and the sample to detector distance was 32.5 cm. A typical measurement time used was 900 s. SAXD and WAXD were collected in $2\theta = 1$–$10°$ and $2\theta = 7$–$55°$ ranges, respectively. One dimensional X-ray diffraction patterns were determined from the 2D images using the GADDS (version 1.28) software. The obtained X-ray diffraction patterns are imported in the Bruker EVA software (version 12.0) for peak identification and peak shape analysis. The average crystal thickness (ACT) was calculated by Scherrer equation based on the Full Width at Half Maximum (FWHM) values of the first order long-spacings of fats from the SAXD spectra. The polymorphism or spatial arrangement of the subcell structure was determined based on peak identification of short-spacings in the WAXD spectra.[42]

Polarized light microscopy

Gels were visualized using a Malvern Morphologi G3S microscope with 10×, 20× and 50× objectives. A small amount of

Published on 08 February 2024. Downloaded on 4/11/2024 2:11:41 PM.

sample was placed onto a microscope slide, thinly spread, and sandwiched with a cover slip. Images were acquired using the polarized mode to enable visualization of the lipid crystal network which displays birefringence unlike amorphous silica.

Confocal laser scanning microscopy

To allow visualization of the double gels, only fumed silica particles and the oil phase were labelled with Nile red at a final concentration of 80 μmol L^{-1}. A Zeiss CLSM with a 63× oil-immersion objective (N.A. = 1.4) is used to characterize the structure of the gels. Silica appears labeled as deep red (in single channel visualization) or yellow orange (in double channel visualization due to colocalization of oil and silica), whereas oil and tripalmitin appear labelled as green and black (*i.e.*, negatively stained) respectively. Silica and oil were detected using two different excitation wavelengths: 488 nm and 633 nm. Intensity data were collected at emission wavelength ranges of 517–624 nm and 660–750 nm for each excitation wavelength, respectively.

Additional images were also collected using an airy scan mode for better visualization at zoom ≥ 2. The Zeiss Airyscan mode converts a diffraction-limited, point-scanning confocal microscope into a super-resolution microscope using a specialized 32-channel Airyscan detector that improves resolution and signal-to-noise ratio.[43]

Images were collected at low $\phi_{\text{tripalmitin}}$ since higher densities gels preclude image acquisition due to multiple scattering and shadowing resulting in poor signal. 2D and z-stacks were acquired at a rate of 1 image per s, at heights $z \gtrsim 5$ μm away from the glass slide, and maximum depth of ~ 20 μm. z-Stacks were reconstructed into 3D images. Image analysis of the 2D images from the z-stack were performed using image processing according to the following steps: (1) enhance image contrast by allowing saturation of 0.2% of pixels, (2) apply a spatial bandpass filter which smooths the image and subtracts background off. The filter allows feature sizes, in pixels, above a 'minimum' average aggregate size of $\gtrsim$1–2 μm for silica aerogels[32] and tripalmitin gels[5] namely obtained from scattering experiments, (3) multiply by a Hanning window to remove edge artifacts that could arise from (4) Fast Fourier Transform (FFT) the windowed image, (5) radially average the Fourier space to obtain the spectrum $I(q)$. The wave vector q represents a spatial frequency, that is a function of the distance from the center in the Fourier space and of the image size converted to μm. The variations of $I(q)$ was described by the characteristic spatial frequency q_c related to the characteristic average cluster size of the network in the real space by $\xi_c = 2\pi/q_c$.[44]

Mechanical characterization

Compression tests

Compression tests were conducted using a Zwick Roell testing system at a constant speed of 0.1 mm s^{-1}. Specimens were compressed a maximum of 0.8 mm. Force–displacement curves were converted to stress–strain curves considering area and initial height of the specimens. The Young moduli were approximated as the slope of the lower portion of the strain–stress curve from the second loading cycle. The first loading cycle was applied to ensure specimens had nearly flat top surface prior to testing.

Rheology

Oscillatory shear viscoelastic moduli and yielding were investigated using frequency sweeps (ω = 0.1–100 rad s^{-1}) and strain sweeps (γ_0 = 0.001–1000%, ω = 2 rad s^{-1}) respectively, in a rotational torque-controlled rheometer (MCR 301, Anton Paar). Thermal behavior was investigated by heating and cooling the Peltier units at the corresponding gelation rate. Samples were carefully loaded onto parallel-plate fixtures with radius R = 10–60 mm (smaller plate diameters were used for stiffer gel samples), which were previously covered with adhesive-back sandpaper (600 grit) to minimize wall slip. A gap height $h \approx$ 400–600 μm was used for all measurements after carefully transferring samples onto the rheometer plate. Varying gap and geometry diameter yielded comparably qualitative results and hence did not influence our findings. A concentric cylinder was used to measure the rheology of the more dilute silica gels ϕ = 0.01–0.02. Elastic moduli were determined within the linear regime (γ_0 = 0.01%), and 'critical' yield strains γ_c and yield stresses σ_c were determined at the onset of yielding where the linear elastic modulus drops by five percent, *i.e.*, $0.95G'_0 = \sigma_c/\gamma_c$, and 'absolute' yield strains γ_{abs} and yield stresses σ_{abs} and stresses were determined at the cross-over point $G' = G''$ (from the intersection of cubic spline fits to G' and G''). Creep tests were conducted by inputting a wide range of stresses σ over sufficient time to induce material fluidization, while recording the accumulated strain γ.

Results and discussion

Aggregation of the gels was achieved by sequential gelation by which the first silica gel network precedes the aggregation of the second tripalmitin gel network (Fig. 1a). To this end, we mixed and equilibrated a three-component system at high temperature T = 75 °C. The ternary system contained a pre-existing silica network at fixed volume fraction: ϕ_{silica} = 0.01, approximately equivalent to the minimum concentration to reach a volume-spanning network as indicated by a measurable finite yield stress $\sigma_y \approx$ 0.5 Pa (Fig. S2, ESI†), dispersed in a triglyceride mixture made of tripalmitin at increasing volume fraction $\phi_{\text{tripalmitin}}$ = 0.03–0.18 and soybean oil. This leads to double gels with increasingly asymmetric mixture composition. Quenching was then performed by lowering the temperature to 5 °C well below the solid–liquid phase transition ($T_m \approx$ 48–58 °C), to enable aggregation of tripalmitin gel within the pre-existing silica network. As gels are metastable amorphous solids, their structure is highly coupled to their thermal history. Aggregation ensued for several days to ensure complete gelation. To demonstrate the thermal responsiveness of the gels, we present a temperature sweep for a representative double gel,

 This journal is © The Royal Society of Chemistry 2024

Published on 08 February 2024. Downloaded on 4/11/2024 2:11:41 PM.

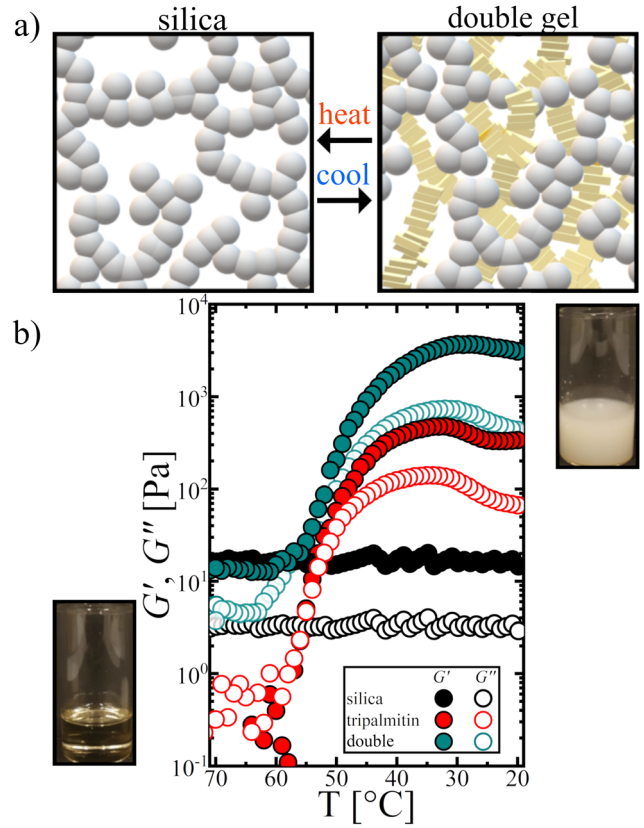

Fig. 1 (a) Schematic representation of a single gel (silica: sphere) dispersed in a mixture of liquid soybean oil and tripalmitin (white background) after melting (left-side), and of a double gel of two interpenetrating particle networks (silica: sphere, tripalmitin: platelet) dispersed in soybean oil before melting (right-side), respectively. Colloidal particles are not monodispersed and are not drawn to scale. Schematic does not reflect the exact multi-length scale structure of silica, and tripalmitin or their combination in double gels. (b) Macroscopic appearance of tripalmitin single gel and double gels are similar and are displayed after melting (left: translucent) and before melting (right: opaque). Silica single gels appear translucent throughout the temperature range. Viscoelastic moduli of single gels and double gels as a function of temperature. Particle concentrations are ϕ_{silica} = 0.01, and $\phi_{tripalmitin}$ = 0.05, and $\phi_{double\ gel}$ = 0.05. Oscillatory measurements were conducted at 2 rad s^{-1}.

ϕ_{silica} = 0.01, $\phi_{double\ gel}$ = 0.05 (Fig. 1b). During heating at $T \gtrsim$ 35 °C, the viscoelastic moduli G' and G'' drop as the tripalmitin crystal network, for both single gels and double gels, begins to melt and disintegrates at $T \gtrsim$ 55 °C. At higher temperatures, elasticity is dominated by the silica network ($G'_{double\ gel}$, $T \gtrsim$ 55 °C $\sim G'_{silica}$ at ϕ_{silica} = 0.01) only for double gels, whereas single gels become viscoelastic fluids.

A key drive for understanding the structure and function of soft materials is to identify a suitable application that translates their properties from the nano-micro scales to the macroscale. Therefore, we assessed the ability of the colloidal double gel inks to construct 3D structures using direct-ink writing.

Fig. 2 demonstrates that the inks retain their shape when extruded through the nozzle (Fig. 2a) and can be assembled into multiple self-supported patterned structures namely solid cylinders (Fig. 2b), multi-walled cylinder (Fig. 2c), and mesh (Fig. 2d). This contrasts with polymeric materials where swelling can occur due to shear-induced alignment leading to printing defects. The printed structures displayed good resolution equivalent to the nozzle size ($\sim$400 μm line width, Fig. 2a), exhibited adequate structural consistency, that is multiple stacked layers were deposited without observing printing defects such as buckling or sagging. Solid cylinders (Fig. 2b) of single gels and double gels were subjected to compression and their mechanics were compared at a fixed total 'printable' volume fraction ϕ = 0.10 (Fig. 2e). Comparing the loading strain–stress curves reveals that the maximum stress during compression σ_{max} of double gels falls in between that of the single gels. Estimation of the moduli yielded closer moduli for silica single gels and double gels: E = 39.0 ± 0.9 kPa and 38.7 ± 1.1 kPa respectively, but not for tripalmitin single gels E = 29.3 ± 0.3 kPa (Fig. S1, ESI†).

While understanding the mechanical properties of double gels has the potential to unveil ways of controlling them, as of now, it remains an open question. Therefore, we investigated the shear oscillatory and creep rheology of colloidal gels in a wide range of volume fractions that reflect increasingly asymmetric mixture compositions and characterize their microstructure to gain further intuition on their mechanical behavior (Fig. 3–7). We place a special emphasis on the mechanics of lipid single gels and double gels, as the volume fraction of silica, ϕ_{silica} = 0.01, is constant in all double gel compositions. Furthermore, emphasis is placed on the dilute regime ($\phi \lesssim$ 0.1), which is better suited for description by models that consider the fractal nature of gels and for establishing a connection between rheology and structure.

Oscillatory shear

Frequency dependence of the viscoelastic moduli reveal that elastic contributions dominate viscous contributions $G' > G''$ in a broad range of timescales as expected for solid-like materials.[45] Particle-concentration dependence (Fig. 3a) of the linear modulus reveals that gels conform to power-law scaling $G'_0 \sim \phi^n$. Such scaling has been linked to a gelation mechanism based on the aggregation of self-similar 'fractal' clusters that dominated the elastic properties of the investigated system.[6,9] The values of the exponents $\sim$4 and $\sim$5 for silica and tripalmitin single gels respectively, are in good agreement with previous findings on low-concentration gels of (i) octadecyl-coated silica particles dispersed in hexadecane (n = 3.6 ± 0.9 at 22 °C) and (ii) tristearin dispersed in olive oil (n = 4.1± 0.9 at 22 °C).[46] While one scaling regime is observed for silica single gels due to strong-link behavior, two regimes are observed for lipid single gels and double gels due to a transition from strong-link to weak-link behavior as a function of ϕ.[15,46,47] Moreover, double gels display similar scaling exponent tripalmitin single gels indicating that the lipid network dominates the linear bulk response at same particle volume fraction. Treating all microstructures as a collection of fractal flocs closely packed throughout the sample, the scaling of the linear elastic modulus with volume fraction is interpreted by fractal

Published on 08 February 2024. Downloaded on 4/11/2024 2:11:41 PM.

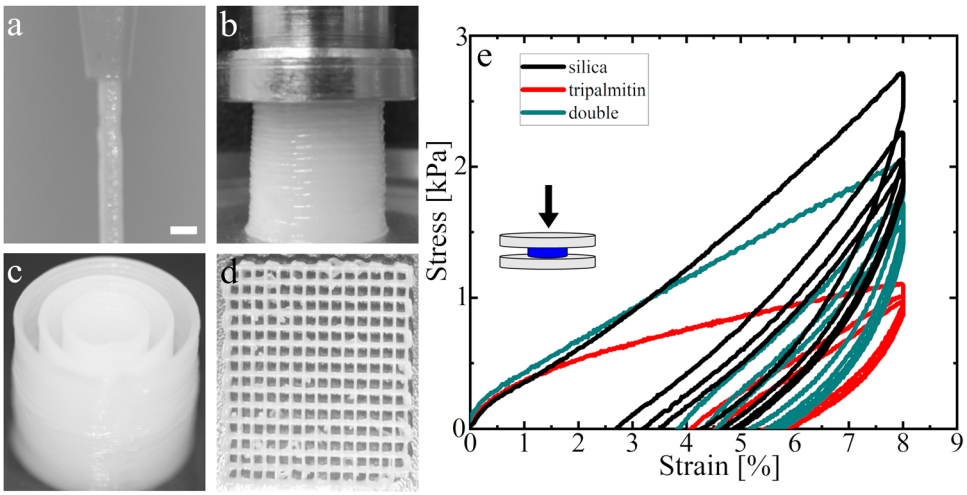

Fig. 2 3D printing of gels at total volume fraction ϕ = 0.10. (a) Diameter of double gel at the exit of the printing nozzle corresponding to the inner nozzle diameter, scale bar = 440 μm. (b), (c) and (d) Examples of 3D-printed shapes: filled solid cylinder (height = 10 mm) used for compression, multiwalled cylinder (height = 10 mm), and mesh illustrating the 'printability' of double gels. Similar printing characteristics were found for single lipid gels provided that ϕ were matched with similar ϕ. (e) Loading and unloading curves of representative single gel and double gel cylinders at similar total volume fraction ϕ = 0.10 of tripalmitin and silica. Double gels comprise ϕ_{silica} = 0.01 and $\phi_{tripalmitin}$ = 0.09, to account for the total volume fraction ϕ = 0.10.

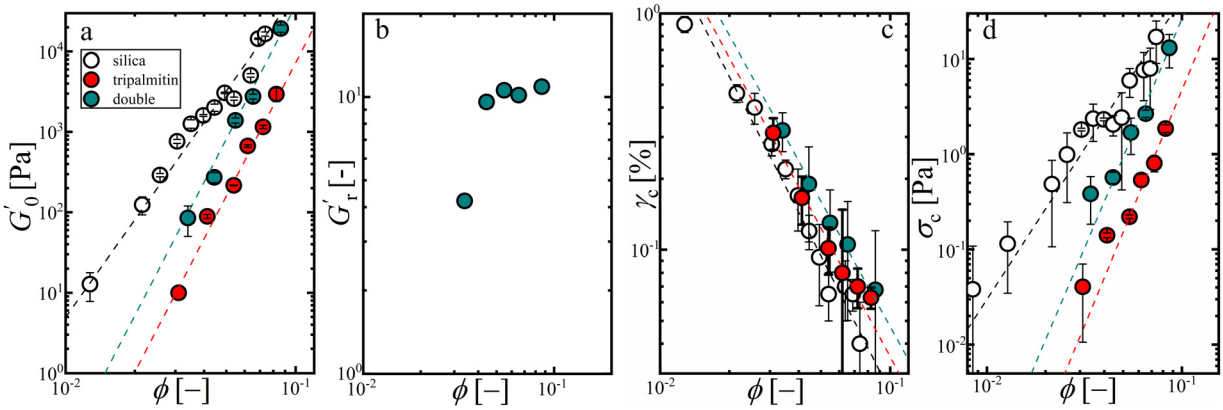

Fig. 3 Shear rheological properties of single gels and double gel as a function of total volume fraction $\phi = \phi_{silica} + \phi_{tripalmitin}$. (a) Linear modulus G_0', (b) non-dimensional relative modulus $G_r' = G_0'$ double gel experimental$/G_0'$ double gel springs-in-parallel (see eqn (2)), (c) critical strain γ_c and associated (d) critical stress σ_c at the onset of yielding $0.95G_0' = \sigma_c/\gamma_c$. Data points with error bars represent averaged quantities with their corresponding standard deviations. Dashed lines are power-law fits to each data set: silica single gels, lipid single gels, and double gels.

theories developed for single colloidal gels in the strong-link and weak-link regimes, irrespective of the shape of the gel's constituent particles.[31] We based our assumptions on past work supporting the utility of such phenomenological models to described the linear oscillatory rheology of lipid and silica gels, while noticing that power-law rheology could also emerge from non-affine reversible arrangements induced by linear perturbations.[6,10,46] In the low-concentration regime ($\phi \lesssim$ 0.1), the interfloc links are stronger than the flocs, and hence the macroscopic elastic constant or elastic moduli is dominated by the flocs. The linear elastic modulus in this regime scales with volume according to:[9,13]

$$G_0' \sim a\phi^{[(d+x)/(d-D)]} \quad (1)$$

where a is a prefactor in Pa that contains the particle elastic constant of a particle of certain size, d the Euclidean dimension, x is the backbone fractal dimension of the crystals and D the fractal dimension of the crystals. The D describes the spatial-dependence of the interconnection between fractal clusters, whereas x describes the spatial-dependence of the contour length of individual fractal chain of particles within the cluster.[11] In using the relationship in eqn (1), we do not estimate the elastic constant of the floc, and assume that d = 3, *i.e.*, the volume occupied, and x = 1–1.3, deducted from theory and experiments on spherical fractal gels.[8,9,11] Solving eqn (1) with scaling exponents of 5 and 4 leads to fractal dimensions of D = 2.1–2.2 for lipid single gels and double gels, and D = 1.9–2 for silica single gels, in good agreement with values reported in the literature.[15,46–49]

 This journal is © The Royal Society of Chemistry 2024

Published on 08 February 2024. Downloaded on 4/11/2024 2:11:41 PM.

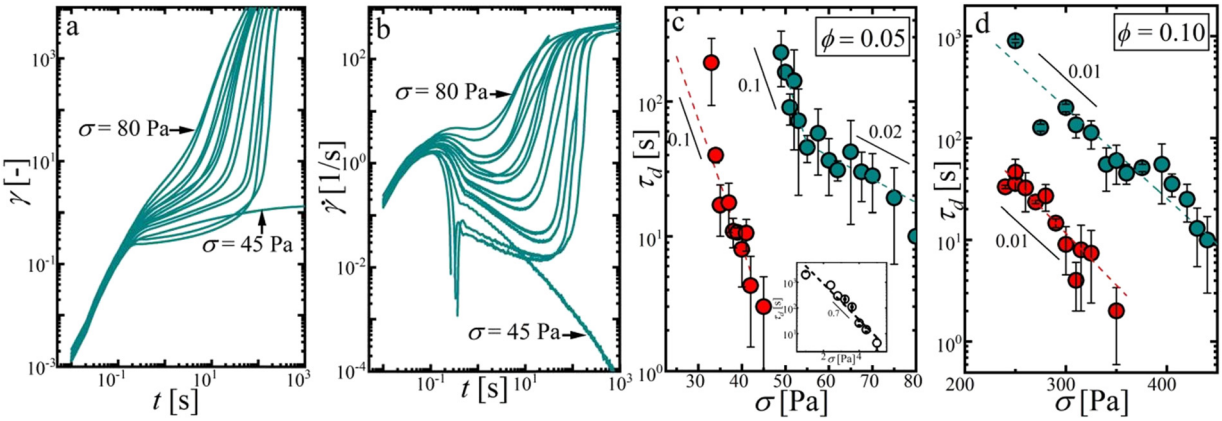

Fig. 4 Illustration of (a) Creep response of double gels at ϕ = 0.05 for σ = 45–80 Pa, increasing stress input right to left to right and (b) corresponding shear rate $\dot{\gamma}$, arrows illustrate the choice for τ_d as the maximum in d$\dot{\gamma}$/dt. (c) and (d) Delay time τ_d between the application of the shear stress and the moment of yield for dilute gels (c) and at the intersection of the dilute-dense regime limit (d). Inset in (c) displays τ_d at fixed ϕ = 0.01. Lines are experimental fits to eqn (4), and slops indicate the scaling of τ_d. Data points with error bars represent averaged quantities with their corresponding standard deviations.

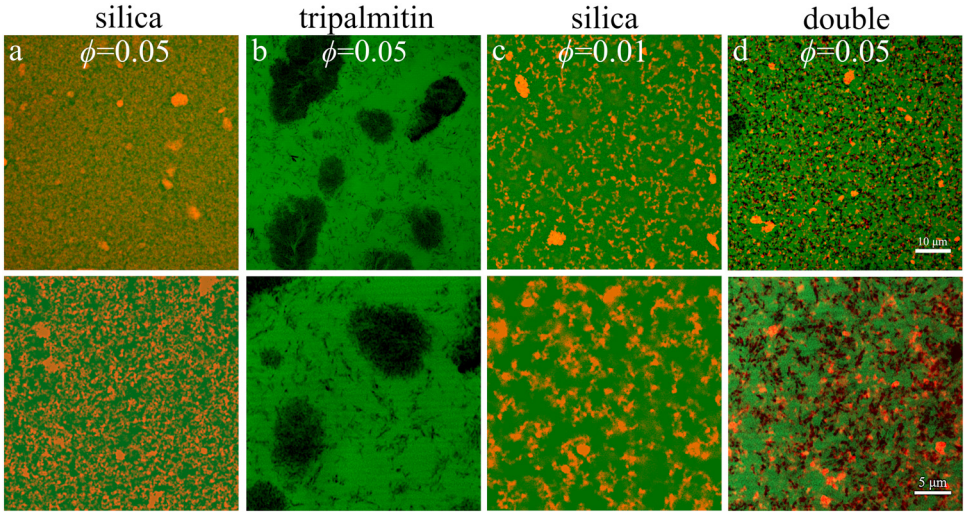

Fig. 5 CLSM images of (a)–(c) single gels and (d) double gels at representative particle volume fractions. Micrographs were acquired with an oil-immersion 63× magnification objective, zoomed 2× (top panel) and 3× (bottom panel). Oil, silica and tripalmitin are assigned false colours: green, red (visualized as orange due to colocalization of the oil and silica channels) and black (negatively-stained) respectively to aid visualization.

A recent study suggests that the elastic modulus of gels made up of two types of colloidal species may be approximate by constitute equation of springs connected in parallel:[21]

$$G_0' \approx \sum_s c_s G_{0,s}' \quad (2)$$

In this, the total elastic constant is approximate as the linear elastic moduli G_0' and is given by sum of the linear elastic moduli $G_{0,s}'$ of each colloidal specie times its mixture composition $c_s = \phi_s/\phi_{tot}$, where ϕ_s corresponds to volume fraction of each 'isolated' specie s, and ϕ_{tot} refers to the total volume fraction. Remarkably, we observe that such model underestimates the modulus by approximately up to an order of magnitude but comes to close experimental agreement at $\phi \gtrsim 0.1$ as $c_{silica} \to 0$ (Fig. S3, ESI†). The observed stiffening at $\phi \lesssim 0.1$ suggests shear-activated cooperative effects resultant from intertwining of the silica-lipid aggregates even at small shear perturbations.

Next, we draw comparisons on the nonlinear rheology of the gels as measured by the onset of yielding (where G' begins to drop) and the point of fluidization (at the crossover $G' = G''$) (Fig. 3c, d and Fig. S2, ESI†). Expectedly, single, and double gels strain-soften corresponding to the most general response of colloidal gels. As ϕ increases, the limit of linearity decreases for all colloidal gels. The scaling of the limit of linearity $\gamma_c \sim \phi^n$ remains comparable for all colloidal gels. We interpret the scaling of the critical strain with volume fraction using similar theories developed for colloidal gels in the strong-link regime:[9,13]

$$\gamma_c \sim a\phi^{-(1+x)/(d-D)} \quad (3)$$

Published on 08 February 2024. Downloaded on 4/11/2024 2:11:41 PM.

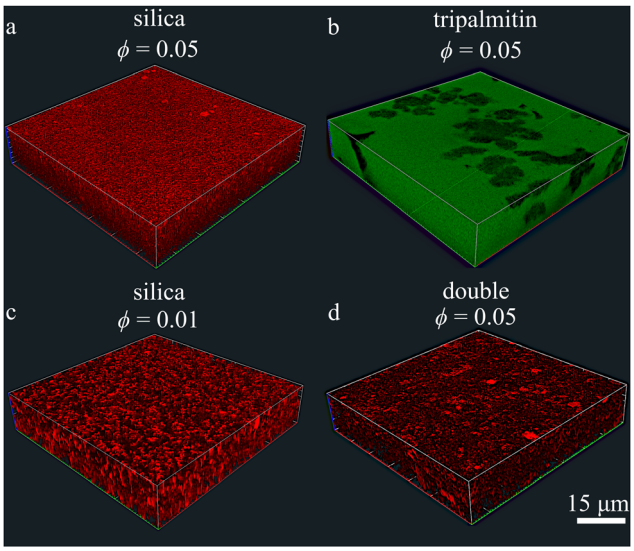

Fig. 6 CLSM z-stacks of (a)–(c) single gels and (d) double gels at representative particle volume fractions, like those displayed in Fig. 5. z-Stacks were acquired with an oil-immersion 63× magnification objective, zoomed 2×. Oil, silica and tripalmitin are assigned false colors: green, red and black (negatively stained) respectively, to aid visualization. For better visualization of the silica gel network, the oil channel has been removed in figures (a), (c), and (d), but not in figure (b).

Using eqn (3) with n = 1.9 and n = 1.8 yields D = 1.8–2 for silica and D = 1.7–1.9 for lipid single gels and double gels. These values are comparable to those obtained from the scaling of the elastic moduli $G_0' \sim \phi^n$. Remarkably, when we quantify the stress at the limit of linearity σ_c and at the cross- over point σ_{abs}, we observe that double gels bear much larger shear stresses than single gels in the dilute regime (Fig. 3 and Fig. S3, ESI†). Such behavior vanishes in the concentrated regime as also observed for $G_0' \sim \phi^n$ (Fig. S3, ESI†).

To further explore this behavior, we probed the dynamics of delayed yielding by creep experiments, *i.e.*, applying stress steps and measuring deformation over time.

Delayed yielding

Tuning the mesoscale structure of colloidal gels holds the potential to not only tune the elastic properties of colloidal gels, but also their failure when subjected to shear stresses. Several studies have shown that delayed yielding or fluidization of gels is governed by association and dissociation dynamics of interparticle bonds forming single gel strands, and strand density forming the macroscopic scale. This response can be modified for instance by tailoring the chemistry of colloidal particles, volume fraction, shear, and quench history, which all dictate gel microstructure.[35] In our study, we tuned the gel mesoscale and sought to make gels more resilient to yielding by introducing the paradigm of interpenetrating double colloidal gels. We performed creep tests on single gels and double gels at selected gel volume fractions encompassing the two mixture

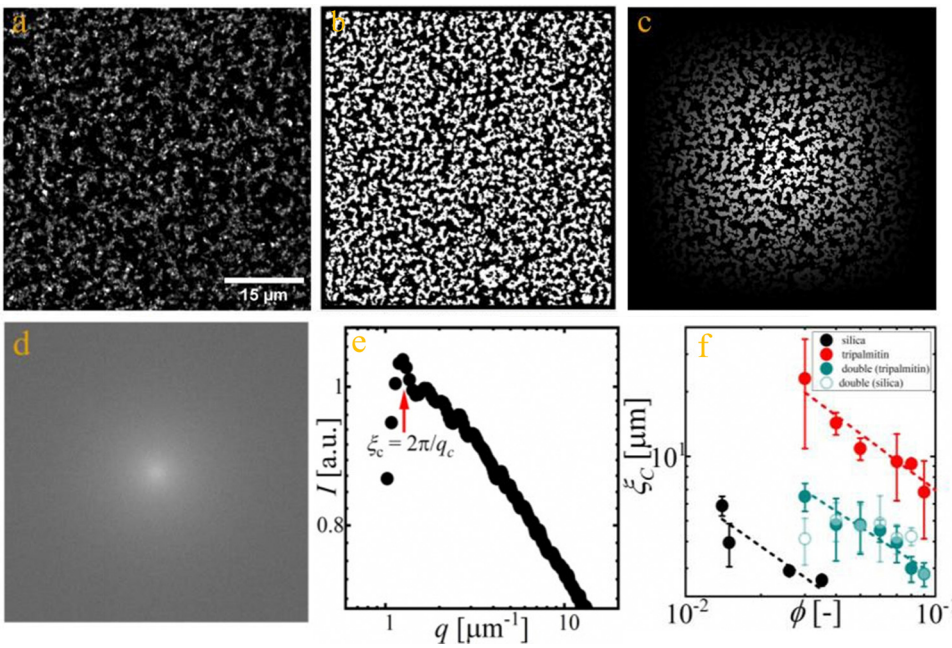

Fig. 7 Steps for image analysis, using a silica gel at ϕ = 0.01 as an example. (a) Raw image allowing 0.2 saturation of pixels to enhance contrast; (b) resulting image after applying a spatial bandpass filter; (c) Hanning window of the image (d) fast Fourier transform of the image, (e) radially-averaged Fourier transform denoting intensity I *vs.* spatial vector q, and indicating the characteristic length-scale or average cluster size ξ_c at which I is maximum. (f) Calculated ξ_c for silica and lipid single gels, and double gels as a function of each gel volume fraction. For double gels, ϕ corresponds to ϕ_{tri} since ϕ_{sil} remains constant. Scaling of average cluster size $\xi_c \sim \phi^n$ is represented by dotted lines where $n \approx -1$. Green solid symbols correspond to the lipid gel component of the double gels, whereas green open symbols correspond to the silica gel component within the double gels. Only solid symbols are used for fitting. Data points with error bars represent averaged quantities with their corresponding standard deviations.

 This journal is © The Royal Society of Chemistry 2024

Published on 08 February 2024. Downloaded on 4/11/2024 2:11:41 PM.

composition regimes. Overall, we observe similar qualitative behavior across samples. For very low σ, the initial creep response is purely elastic: increases linearly with time, ensued by inertio-elastic oscillations after which γ becomes nearly independent of time (Fig. 4a) and $\dot{\gamma}$ tends to zero (4(b)). Virtually little to no creep is observed during the length of the experiment. However, as σ increases, the initial response remains the same, but the time-independent creep response persists only for a finite time, after which the sample fails catastrophically and both γ and $\dot{\gamma}$ increase steadily (Fig. 4a and b). This occurs after a delay time τ_d, taken as the maximum in $d\dot{\gamma}/dt$. As σ increases further τ_d decreases, and eventually failure becomes nearly instantaneous signaled by very narrow time-independent creep and very low τ_d values. We further visualize the effect of ϕ on the dynamics of yielding by plotting τ_d as a function of σ on a semilogarithmic scale. We observed that τ_d decays exponentially over the probed σ range as observed in other single colloidal gels.[35] We note that for $\phi \lesssim 0.1$ double gels but no lipid single gels display a double exponential dependence of the yield time on the stress. The presence of the two exponential regimes in these systems has been ascribed to simultaneous dissociation of multiple interparticle bonds in thick force-bearing strands, which leads to rupture of the entire strands. Whereas, a single exponential regime is attributed to thin force-bearing strands, in which rearrangements on single-particle scales alone can trigger mesoscopic and macroscopic deformations. Applying a mean-field bond rupture model, the delayed yielding dynamics can be captured:[50]

$$\tau_d \approx \begin{cases} \dfrac{1}{n^2 \sigma C k_A}\left(\dfrac{k_A}{k_D}\right)^n e^{-n\sigma C}, & k_D \ll k_A \\ \dfrac{S_n}{\sigma C k_D} e^{-\sigma C}, & k_D \gg k_A \end{cases} \quad (4)$$

where, τ_d is the time representing the slow erosion of the macroscopic scale of a colloidal gel. This length-scale, comprises a total area density of strands ρ with n individual bonds within each single strand. The model also considers the reassociation of entire gel strands as negligible $K_A = 0$ compared to their dissociation rate K_D, which increases exponentially as σ increases. The parameter $C = \delta/n\rho_0 k_B T$ has the units of compliance, and σC denotes the elastic energy per bond at yield. The ratio of the characteristic stresses for each regime is determined by the number of bonds across a strand n. The two stress regimes of τ_d at a critical stress $\sigma_c = C^{-1}\ln(k_A/k_D)$, at which bond rupture and healing occur at the same rate $k_D = k_A$. The microscopic parameter C sets the order of magnitude for the relevant stresses for the delayed yield. All structural parameters are obtained directly from the slope and intercepts from the exponential regimes. Taking as example double gels at $\phi = 0.05$, the slope of the high stress regime directly yields $C = 1.8 \times 10^{-2}$ Pa^{-1}, and thus the slope nC of the low stress regime yields $n = 5.8$. From the extrapolation of τ_d to σ_0 for each regime, we find $k_D = 1.3 \times 10^{-1}$ s^{-1} and $k_A = 3.7 \times 10^{-1}$ s^{-1}. From this, we estimated the crossover critical stress $\sigma_c = 56$ Pa. Remarkably, at $\phi \lesssim 0.1$, while we observed two exponential decay regimes for double gels, whereas only one for lipid single gels. At higher volume fractions $\phi \gtrsim 0.1$, a single exponential regime is observed for all gels as erosion is increasingly controlled entirely by the lipid crystal network as highlighted by similar decaying exponentials and comparable τ_d (see Fig. 4d and Fig. S4, ESI†). All structural parameters for the various gel systems obtained from the model are summarized in Table S1 (ESI†). Overall, at $\phi \lesssim 0.1$, the increase in the ratio of the slopes from $n \approx 1$ to $n \approx 5$ supports the notion of thicker gels strands undergoing yielding in double gel networks and highlights their pivotal role in modulating the flow response.

Interplay between structure and rheology

To discard any changes on the packing or thickness of lipid crystalline nanoplatelets, wide-angle and small-angle X-ray diffraction experiments were conducted. These confirm that all structural changes, if any, would occur at microscopic-to-mesoscopic length scales (see Fig. S4, ESI†). To infer on the structural origins of the unusual mechanics, we visualize the static mesoscopic structure of tripalmitin single gels, silica single gels and double gels (Fig. 5–7, and Fig. S5–S7, ESI†). Under polarized microscopy, we observe that tripalmitin single gels and double gels display birefringence due to the presence of crystalline aggregates in contrast to the amorphous silica gels. Moreover, double gels are composed of lipid clusters that appear on average smaller than those of lipid single gels (Fig. S5 and S6, ESI†). To investigate further this behavior, we collected CLSM micrographs that selectively display morphological features due to fluorescence arising from silica and the liquid oil and preserves the integrity of the sample as it does not requires spreading of a thin film like PLM (Fig. 5 and 6). At $\phi \lesssim 0.1$, the pre-existing silica network appears to promote dense double gel networks devoid of large clusters. In contrast lipid single gels display large clusters ($\gtrsim 5$ μm), seemingly linked by smaller aggregates. At $\phi \gtrsim 0.1$, such effect reasonably vanishes as the silica network becomes too soft, and double gels resemble pure lipid single gels (Fig. S7, ESI†) in terms of composition: $c_{silica} \to 0$, consistent with rheological measures. To quantify these differences, we computed the average characteristic length-scale ξ_c, often considered as an average cluster size at intermediate length scale where fractal gels are inhomogeneous (Fig. 7). The characteristic cluster size decreases with increasing volume fraction according to $\xi_c \sim \phi^{1/(D-3)}$.[9] Substituting with an average fractal dimension $D = 2$ deducted from rheological measurements for all gels, nearly accounts for the scaling $n \approx -1$ observed experimentally (Fig. 7f). Interestingly, while the scaling remains comparable, ξ_c of the lipid gel network in double gels is lower than that in lipid single gels for all volume fractions but closer to ξ_c of silica gels at $\phi = 0.01$. The latter suggests that the primer silica network sets the physical length-scale of the latter aggregated lipid network in double gels. Smaller ξ_c means aggregates that are more densely-packed, and homogeneously interconnected within the gel network, which could lead to more robust and stiffer gels. Other mechanisms such as hindered particle rotation due to interpenetration in double gels could further reinforce gel

Published on 08 February 2024. Downloaded on 4/11/2024 2:11:41 PM.

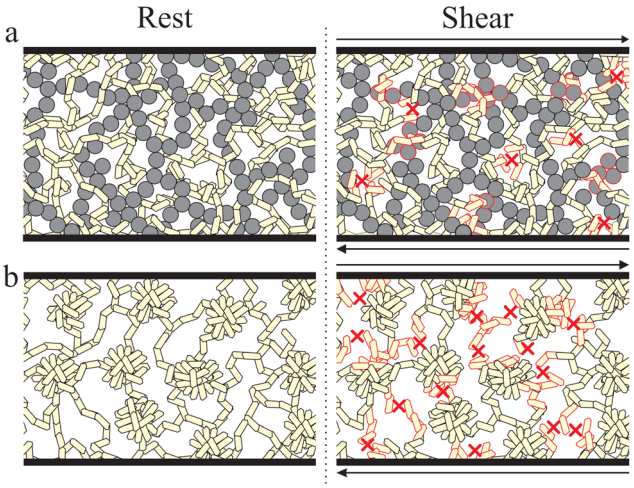

Fig. 8 Schematic illustration of suggested stiffening/yielding mechanism of (a) double gels *versus* (b) lipid single gels at rest (left-side) and during shear (right-side). Spheres: silica and platelets: tripalmitin. Arrows indicate the direction of the applied shear stress. During shear, red outlines in some particle aggregates and red crosses indicate "weak-links" where aggregates deform and in some cases break, respectively. In double gels (top row), particle aggregates are less prone to deformation and failure (less red-contoured particles and less red crosses), due to more uniformly spaced, denser, and interpenetrated networks. In single gels (bottom row), particle aggregates are more susceptible to deformation and breakage (more red-contoured particles and more red crosses) due to more heterogeneous larger clusters connected by thinner gel strands. Colloidal particles are not monodispersed and are not drawn to scale. Schematics do not reflect the exact geometry, size, or volume fraction of the particles.

networks during yielding in analogy to what is observed for gel networks made of "rough" and "less mobile" single colloidal aggregates.[16,24,51]

Taking together our experimental findings, we propose that double gels tend to be more resilient and harder to yield, as interpenetration of gel networks lead to densely packed and more interconnected structures. Such structures remain more elastic as gel clusters are much less able to align under shear flow and experience large non-affine deformations (Fig. 8). While it is experimentally challenging to quantify these microscopic effects during yielding in the current systems, recent computer simulations involving colloidal double gels provide support for such a scenario.[10] Future studies using structural and rheological probes are further needed to interrogate the static and dynamic structure of double gels and elucidate cooperative effects between the two gel networks under step-controlled experiments and large-amplitude oscillatory shear.

Conclusions

In conclusion, our study demonstrates a new paradigm in the design of soft materials: oil- continuous double gels made of interpenetrating networks from colloidal particles. Double gels are sequentially-assembled, thermo-responsive and present good resolution and structural consistency in 3D-printed constructs. In the dilute regime $\phi \lesssim 0.1$, double gels display much larger stiffness and enhanced yielding response when compared to their lipid single gel counterparts, not accounted by simple additive elastic effects of the gel networks. A plausible mechanism for the enhanced mechanical response of double gels is the decrease in the characteristic length-scale or correlation length indicating more densely-packed and spatially homogeneous gels, due to steric hindrance of the interpenetrating networks. The approach presented here could be broadly generalized to the assembly of alkane-based colloids in apolar solvents and oils in which short-range attractive interactions can be thermally activated such as wax-based gels, in presence of another colloidal gel.

This versatility makes double gels interesting candidates for a multitude of potential applications in lipid structuring of foods, consumer products and additive manufacturing of various soft materials.

Conflicts of interest

The authors declare no competing financial interest or conflicts of interest.

Acknowledgements

The authors thank Patricia Heussen and Daan Giesen for technical support in CLSM imaging and 3D printing, respectively. This project has received funding from the European Union's Horizon 2020 research and innovation programme under the Marie Sokolowski-Curie grant agreement no. 798917.

References

1 J.-L. Barrat, E. Del Gado, S. U. Egelhaaf, X. Mao, M. Dijkstra, D. J. Pine, S. K. Kumar, K. Bishop, O. Gang, A. Obermeyer, C. M. Papadakis, C. Tsitsilianis, I. I. Smalyukh, A. Hourlier-Fargette, S. Andrieux, W. Drenckhan, N. Wagner, R. P. Murphy, E. R. Weeks, R. Cerbino, Y. Han, L. Cipelletti, L. Ramos, W. C. K. Poon, J. A. Richards, I. Cohen, E. M. Furst, A. Nelson, S. L. Craig, R. Ganapathy, A. K. Sood, F. Sciortino, M. Mungan, S. Sastry, C. Scheibner, M. Fruchart, V. Vitelli, S. A. Ridout, M. Stern, I. Tah, G. Zhang, A. J. Liu, C. O. Osuji, Y. Xu, H. M. Shewan, J. R. Stokes, M. Merkel, P. Ronceray, J.-F. Rupprecht, O. Matsarskaia, F. Schreiber, F. Roosen-Runge, M.-E. Aubin-Tam, G. H. Koenderink, R. M. Espinosa-Marzal, J. Yus and J. Kwon, *J. Phys. Mater.*, 2024, 7, 012501.
2 P. J. Lu, E. Zaccarelli, F. Ciulla, A. B. Schofield, F. Sciortino and D. A. Weitz, *Nature*, 2008, **453**, 499–503.
3 F. Sciortino and E. Zaccarelli, *Curr. Opin. Colloid Interface Sci.*, 2017, **30**, 90–96.
4 F. Peyronel, D. A. Pink and A. G. Marangoni, *Curr. Opin. Colloid Interface Sci.*, 2014, **19**, 459–470.
5 F. Peyronel, B. Quinn, A. G. Marangoni and D. A. Pink, *J. Phys.: Condens. Matter*, 2014, **26**, 464110.

 This journal is © The Royal Society of Chemistry 2024

Published on 08 February 2024. Downloaded on 4/11/2024 2:11:41 PM.

6 A. G. Marangoni, J. P. M. van Duynhoven, N. C. Acevedo, R. A. Nicholson and A. R. Patel, *Soft Matter*, 2020, **16**, 289–306.
7 E. van der Linden and E. A. Foegeding, *Modern biopolymer science*, Elsevier, 2009, pp. 29–91.
8 P. Meakin, I. Majid, S. Havlin and H. E. Stanley, *J. Phys. A: Math. Gen.*, 1984, **17**, L975.
9 W.-H. Shih, W. Y. Shih, S.-I. Kim, J. Liu and I. A. Aksay, *Phys. Rev. A: At., Mol., Opt. Phys.*, 1990, **42**, 4772.
10 S. Aime, L. Cipelletti and L. Ramos, *J. Rheol.*, 2018, **62**, 1429–1441.
11 A. Dinsmore and D. Weitz, *J. Phys.: Condens. Matter*, 2002, **14**, 7581.
12 R. Buscall, P. D. Mills, J. W. Goodwin and D. Lawson, *J. Chem. Soc., Faraday Trans. 1*, 1988, **84**, 4249–4260.
13 S. S. Narine and A. G. Marangoni, *Phys. Rev. E: Stat. Phys., Plasmas, Fluids, Relat. Interdiscip. Top.*, 1999, **60**, 6991.
14 P.-K. Kao, M. J. Solomon and M. Ganesan, *Soft Matter*, 2022, **18**, 1350–1363.
15 R. Vreeker, L. Hoekstra, D. Den Boer and W. Agterof, *Colloids Surf.*, 1992, **65**, 185–189.
16 F. J. Müller, L. Isa and J. Vermant, *Nat. Commun.*, 2023, **14**, 5309.
17 E. Bianchi, R. Blaak and C. N. Likos, *Phys. Chem. Chem. Phys.*, 2011, **13**, 6397–6410.
18 B. Liu, Y. Wu and S. Zhao, *Chem. – Eur. J.*, 2018, **24**, 10562–10570.
19 F. Varrato, L. Di Michele, M. Belushkin, N. Dorsaz, S. H. Nathan, E. Eiser and G. Foffi, *Proc. Natl. Acad. Sci. U. S. A.*, 2012, **109**, 19155–19160.
20 L. Di Michele, D. Fiocco, F. Varrato, S. Sastry, E. Eiser and G. Foffi, *Soft Matter*, 2014, **10**, 3633–3648.
21 C. Ferreiro-Córdova, E. Del Gado, G. Foffi and M. Bouzid, *Soft Matter*, 2020, **16**, 4414–4421.
22 F. M. Hecht and A. R. Bausch, *Proc. Natl. Acad. Sci. U. S. A.*, 2016, **113**, 8577–8582.
23 J. N. Immink, J. E. Maris, J. J. Crassous, J. Stenhammar and P. Schurtenberger, *ACS Nano*, 2019, **13**, 3292–3300.
24 G. J. Donley, M. Bantawa and E. Del Gado, *J. Rheol.*, 2022, **66**, 1287–1304.
25 E. Kamio, T. Yasui, Y. Iida, J. P. Gong and H. Matsuyama, *Adv. Mater.*, 2017, **29**, 1704118.
26 H. J. Zhang, T. L. Sun, A. K. Zhang, Y. Ikura, T. Nakajima, T. Nonoyama, T. Kurokawa, O. Ito, H. Ishitobi and J. P. Gong, *Adv. Mater.*, 2016, **28**, 4884–4890.
27 C. Li, M. J. Rowland, Y. Shao, T. Cao, C. Chen, H. Jia, X. Zhou, Z. Yang, O. A. Scherman and D. Liu, *Adv. Mater.*, 2015, **27**, 3298–3304.
28 J.-Y. Sun, X. Zhao, W. R. K. Illeperuma, O. Chaudhuri, K. H. Oh, D. J. Mooney, J. J. Vlassak and Z. Suo, *Nature*, 2012, **489**, 133–136.
29 W. Yang, H. Furukawa and J. P. Gong, *Adv. Mater.*, 2008, **20**, 4499–4503.
30 J. P. Gong, Y. Katsuyama, T. Kurokawa and Y. Osada, *Adv. Mater.*, 2003, **15**, 1155–1158.
31 R. Kiyama, M. Yoshida, T. Nonoyama, T. Sedlačík, H. Jinnai, T. Kurokawa, T. Nakajima and J. P. Gong, *Adv. Mater.*, 2023, **35**, 2208902.
32 A. Mulderig, G. Beaucage, K. Vogtt, H. Jiang and V. Kuppa, *J. Aerosol Sci.*, 2017, **109**, 28–37.
33 R. R. Chauhan, R. P. A. Dullens, K. P. Velikov and D. G. A. L. Aarts, *Food Funct.*, 2017, **8**, 352–359.
34 P. Efsa, M. Younes, P. Aggett, F. Aguilar, R. Crebelli, B. Dusemund, M. Filipič, M. Frutos, P. Galtier and D. Gott, *EFSA J.*, 2018, **16**, e5088.
35 U. FDA, Food and D. Administration, US Food and Drug Administration, Washington, DC, USA, 2018.
36 L. Phipps, *Nature*, 1962, **193**, 541–542.
37 C. P. Whitby, *Front. Sustainable Food Syst.*, 2020, **4**, 585160.
38 A. G. Marangoni, *Phys. Rev. B: Condens. Matter Mater. Phys.*, 2000, **62**, 13951.
39 M. L. Gee and J. N. Israelachvili, *J. Chem. Soc., Faraday Trans.*, 1990, **86**, 4049–4058.
40 E. Lattuada, T. Pietrangeli and F. Sciortino, *J. Chem. Phys.*, 2022, **157**(13), 135101.
41 W. C. K. Poon, E. R. Weeks and C. P. Royall, *Soft Matter*, 2012, **8**, 21–30.
42 A. G. Marangoni, *Structure-function analysis of edible fats*, Elsevier, 2018.
43 X. Wu and J. A. Hammer, *Confocal Microscopy: Methods and Protocols*, Springer, 2021, pp. 111–130.
44 Y. Gao and M. E. Helgeson, *Opt. Express*, 2014, **22**, 10046–10063.
45 B. Macias-Rodriguez and A. G. Marangoni, *Rheol. Acta*, 2016, **55**, 767–779.
46 M. Grant and W. Russel, *Phys. Rev. E: Stat. Phys., Plasmas, Fluids, Relat. Interdiscip. Top.*, 1993, **47**, 2606.
47 T. S. Awad, M. A. Rogers and A. G. Marangoni, *J. Phys. Chem. B*, 2004, **108**, 171–179.
48 N. Dagès, L. V. Bouthier, L. Matthews, S. Manneville, T. Divoux, A. Poulesquen and T. Gibaud, *Soft Matter*, 2022, **18**, 6645–6659.
49 D. A. Pink, F. Peyronel, B. Quinn, P. Singh and A. G. Marangoni, *J. Phys. D: Appl. Phys.*, 2015, **48**, 384003.
50 J. Sprakel, S. B. Lindström, T. E. Kodger and D. A. Weitz, *Phys. Rev. Lett.*, 2011, **106**, 248303.
51 H. T. Nguyen, A. L. Graham, P. H. Koenig and L. D. Gelb, *Soft Matter*, 2020, **16**, 256–269.